Physics of the Solid State, Vol. 47, No. 3, 2005, pp. 531–538. Translated from Fizika Tverdogo Tela, Vol. 47, No. 3, 2005, pp. 512–518.

LATTICE DYNAMICS AND PHASE TRANSITIONS

Vibrational Spectrum and Elastic Properties of KPb_2Cl_5 Crystals

K. S. Aleksandrov*, A. N. Vtyurin*, A. P. Eliseev, N. G. Zamkova*, L. I. Isaenko**, S. N. Krylova*, V. M. Pashkov**, P. P. Turchin***, and A. P. Shebanin****

** Kirensky Institute of Physics, Siberian Division, Russian Academy of Sciences, Akademgorodok, Krasnoyarsk, 660036 Russia*

e-mail: vtyurin@iph.krasn.ru

*** Joint Institute of Geology, Geophysics, and Mineralogy, Siberian Division, Russian Academy of Sciences, pr. Nauki 3, Novosibirsk, 630090 Russia*

**** Krasnoyarsk State University, Krasnoyarsk, 660041 Russia*

Received June 22, 2004

Abstract— The Raman spectra and elastic moduli of KPb_2Cl_5 crystals were studied experimentally. The results are interpreted using a parameter-free model of the crystal lattice dynamics with inclusion of the multipole moments of the electron shells of ions. The calculated and experimental results are in good agreement. It is shown that not only the halogen ions but also the heavy cations make a significant contribution to the eigenvectors of high-frequency lattice vibration modes, which accounts for the relatively low frequencies of these modes. *© 2005 Pleiades Publishing, Inc.*

1. INTRODUCTION

The current development of solid-state systems of infrared nonlinear optics and photonics has stimulated a search for and the creation of new materials that have a broad spectral window in the IR region (the low-frequency boundary is 30 μm). Because of this trend, interest has recently arisen in studying the optical and spectral properties of complex halides containing heavy cations, which have a relatively short phonon spectrum in contrast to traditional oxide systems.

Crystals of the $Me^+Pb_2Hal_5$ family (where Me^+ is an alkali metal and Hal is a halogen) have the abovementioned spectral window in the IR region, and there exist techniques for growing relatively large single crystals of these compositions [1]. Unlike many other complex halides, these crystals are sufficiently resistant to the atmosphere. A rather loose packing of ions having large radii in the lattice opens up wide possibilities for varying the compositions and properties of these crystals and for their use as active laser media [2]. However, the physical properties of these crystals have not been studied in detail.

In this work, we study the vibrational spectrum and elastic properties of KPb_2Cl_5 crystals, which belong to this family. In this study, we intend to elucidate the nature of formation of the low-frequency boundary of the spectral window of the crystal and determine the structural blocks and interactions that control its position. This study also allows us to obtain information on the relation between the crystal structure and the crystal elastic moduli, which are of interest from both the standpoint of materials-science characterization of the material and its possible applications in acoustooptical IR devices.

To interpret the vibrational spectrum and to establish a relation between the lattice vibration frequencies and the lattice structure, we use the first-principles approach developed recently in [3–5]. It should be noted that, in the case of low-symmetry structures with a large number of atoms in a unit cell, the use of empirical methods (see, e.g., [6, 7]), which are traditionally employed for this purpose, requires a large number of fitting parameters, which cannot be determined using a limited amount of experimental data. Therefore, the application of parameter-free methods becomes very important.

2. EXPERIMENTAL

KPb_2Cl_5 crystals belong to the monoclinic space group $P2_1/c$ and have a = 8.854(2) Å, b = 7.927(2) Å, c = 12.485(3) Å, β = 90.05(3), V = 876.3(4) Å^3, Z = 4, and a density of 4.781 g/cm^3. The coordinates of the atoms are given in Table 1, and the projection of the structure on the *bc* plane is shown in Fig. 1 [8].

To fabricate optical-grade single crystals, the starting $PbCl_2$ and KCl reagents were repeatedly purified by resolidification. KPb_2Cl_5 crystals were grown using the Bridgman crystal growth technique in a two-zone furnace. The linear temperature gradient in the growth region of the furnace was about 20 K/cm, and the velocity of ampoule motion to the cold zone was 2–4 mm/day. The technique is described in more detail in [9]. The crystal structure was determined at room temperature using a STOE STADI4 single-crystal diffractometer and MoK_α radiation ($2\theta_{max}$ = 80°). The samples chosen had no inclusions or defects visible under a polarizing microscope and were subjected to a mechanical treat-

Table 1. Atomic coordinates ($\times 10^4$) in crystal KPb_2Cl_5

	X	*Y*	*Z*
K(1)	5092(5)	514(6)	1696(4)
Pb(1)	65(1)	58(1)	1742(1)
Pb(2)	2547(1)	4359(1)	9937(1)
Cl(1)	9585(4)	1655(5)	4023(3)
Cl(2)	2218(4)	405(4)	9986(3)
Cl(3)	5401(5)	1798(6)	4186(4)
Cl(4)	2355(5)	3117(5)	2204(3)
Cl(5)	7702(6)	3449(5)	1885(3)

ment followed by polishing in a solution of hydrochloric acid.

Raman spectra were excited with polarized 514.5-nm radiation from a 500-mW Ar^+ laser. The spectra were recorded on a U-1000 spectrometer (I.S.A. Jobin Yvon, France). For experiments, we used $2 \times 2 \times 4$-mm samples, with the edges orientated along the crystallographic axes.

The elastic moduli $C_{\lambda\mu}$ were determined by measuring the velocities of bulk acoustic waves (BAWs) followed by solving the inverse problem of crystal acoustics.

The BAW velocities were measured using four single-crystal samples in the form of a rectangular parallelepiped with linear dimensions of about 6 mm. The faces of the first sample were normal to the [100], [010], and [001] crystallographic axes. The faces of the other three samples were normal to the axes of the coordinate system that is obtained by rotating the initial system through 45° about one of the following three axes: axis X_1 ([100], $\left[0\frac{1}{\sqrt{2}}\frac{1}{\sqrt{2}}\right]$, $\left[0\frac{-1}{\sqrt{2}}\frac{1}{\sqrt{2}}\right]$ directions), X_2 ($\left[\frac{1}{\sqrt{2}}0\frac{1}{\sqrt{2}}\right]$, [010], $\left[\frac{-1}{\sqrt{2}}0\frac{1}{\sqrt{2}}\right]$ directions), or X_3 ($\left[\frac{1}{\sqrt{2}}\frac{1}{\sqrt{2}}0\right]$, $\left[\frac{-1}{\sqrt{2}}\frac{1}{\sqrt{2}}0\right]$, [001] directions). Using the crystal symmetry and this set of directions, we can perform two independent measurements in different crystallographic directions for each velocity to be measured. X-ray orientations of the samples were carried out to an accuracy of better than ±5'. The opposite faces of the samples were parallel to each other with an accuracy of better than ±2 μm/m.

The velocities of longitudinal and shear BAWs were measured using a pulse ultrasound method [10]; the block diagram of the setup employed is shown in Fig. 2. The operation of the setup is based on measuring the time of propagation of an ultrasound pulse in a sample. A short (10-ns) video pulse from generator *1* is supplied to piezoelectric transducer *2* (the BAW velocities are measured with piezoelectric transducers based on lithium niobate with a resonance frequency of 29.5 MHz); after multiple reflections in sample *3*, a pulse train is preliminarily amplified by amplifier *4* and then is visually recorded by oscilloscope *5*. The main pulse train of time-interval counter *6* activates generator *1*, and the delayed-pulse train synchronizes the sweep of oscillo-

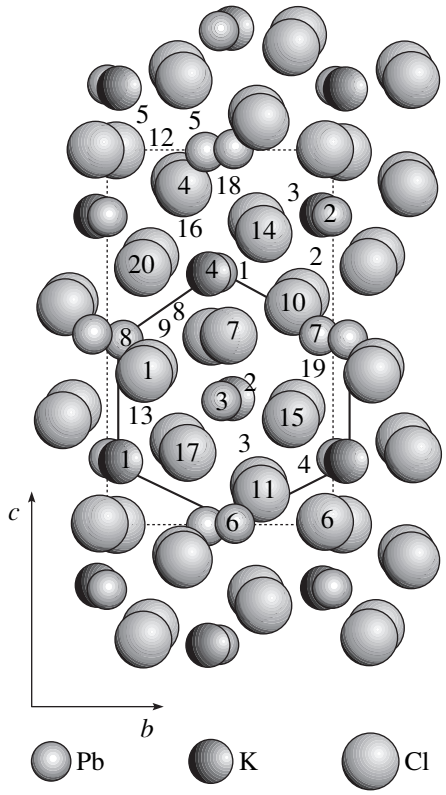

Fig. 1. Projection of the KPb_2Cl_5 structure on the *bc* plane. The pseudohexagonal packing of the channels that contain metal cations and are extended along the *a* direction is shown. Numerals are the ion numbers (identical to those in Fig. 4).

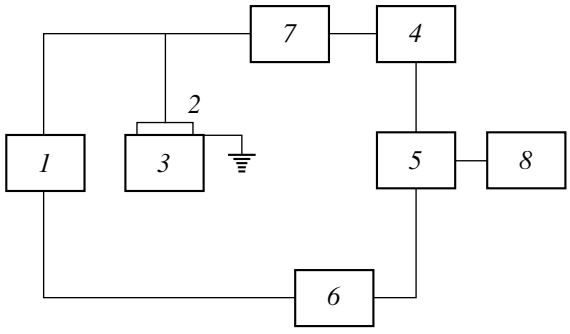

Fig. 2. Block diagram of the ultrasound experimental setup: (*1*) G5-11 video-pulse generator, (*2*) piezoelectric transducer, (*3*) sample, (*4*) U2-5 resonance amplifier (30 MHz), (*5*) S7-9 sampling oscilloscope, (*6*) I2-26 time-interval counter, (*7*) diode limiter of the probe-pulse amplitude, and (*8*) ATsP 1 analog-to-digital converter.

scope 5. The experimental procedure consists in measuring the time interval between two sequentially reflected radio pulses on the oscilloscope screen. This scheme gives an accuracy of 10^{-2} and 10^{-4}% for absolute and relative measurements of the BAW velocities, respectively.

3. RESULTS AND DISCUSSION

3.1. Vibrational Spectrum

The vibrational representation is reduced to the following irreducible representations at the center of the Brillouin zone:

$$\Gamma = 24A_g(xx, yy, zz, xy, yx) + 24B_g(xz, zx, yz, zy) + 24A_u + 24B_u, \quad (1)$$

where the parentheses contain the Raman tensor components for which the corresponding lattice vibrations are active. Note that, because of the low symmetry and the complex crystal structure, it is impossible to separate vibration modes related by individual atomic sublattices using group-theoretical considerations.

The experimental Raman spectra of KPb_2Cl_5 crystals recorded at room temperature are shown in Fig. 3. As expected, the spectra are restricted to low frequencies; indeed, all the lines are below 250 cm^{-1}. The spectra are strongly anisotropic, and the spectral lines are highly polarized. The number of well-resolved peaks is slightly smaller than the number of modes determined from Eq. (1); therefore, their interpretation requires comparison of the peaks with the results of model calculations.

The vibrational spectrum of the KPb_2Cl_5 crystal lattice was calculated in terms of the generalized Gordon–Kim model [3, 4], in which distortions of the electron densities of ions are included. Taking these distortions into account is especially important for low-symmetry structures, since the interactions of multipole moments of ions in them contribute substantially to the total lattice energy and the crystal vibration frequencies.

Following [3, 4], we calculated the electron-density distribution of each ion in the presence of an external field of the corresponding symmetry:

$$V_{\text{ext}}^{(l)} = r^{(l)}P_l(\cos\theta), \quad (2)$$

where $P_l(\cos\theta)$ are Legendre polynomials. The spherically symmetrical component of an external potential was taken to be the Watson sphere potential

$$V_W = \begin{cases} -Z_{\text{ion}}/R_W, & r < R_W \\ -Z_{\text{ion}}/r, & r > R_W. \end{cases} \quad (3)$$

In the calculations, we took into account dipole ($l = 1$) and quadrupole ($l = 2$) electron-density distortions.

The radii of the Watson spheres for each ion were determined by minimizing the total crystal energy

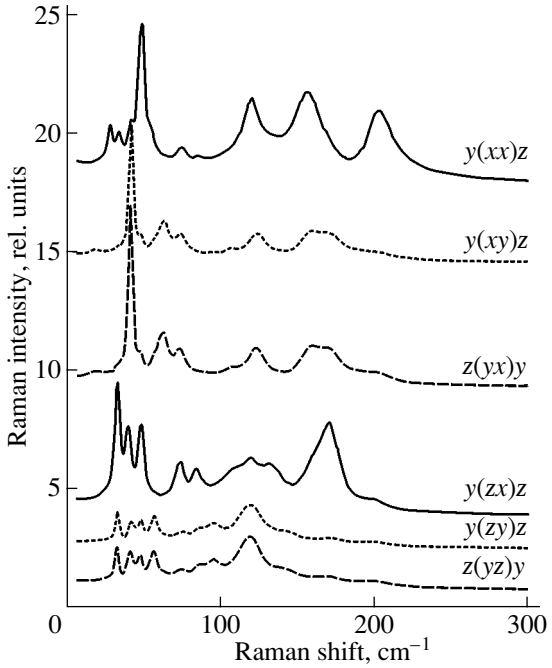

Fig. 3. Polarized Raman spectra of crystal KPb_2Cl_5.

(Table 2). Table 2 also contains the dipole (α_d) and quadrupole (α_q) ion polarizabilities calculated using a modified Steinheimer equation [3, 4]. The corresponding values of induced dipole (P) and quadrupole (Q) moments were found by minimizing the total crystal energy with respect to the corresponding moment: $\partial E/\partial P_\alpha = 0$ and $\partial E/\partial Q_{\alpha\beta} = 0$. The expressions used to calculate the total crystal energy, dipole and quadrupole moments, and the dynamical matrix can be found in [4, 5].

The equilibrium values of the lattice parameters were refined by minimizing the total crystal energy as a function of these parameters. For this purpose, we used the experimentally determined atomic coordinates in the unit cell (Table 1). The values obtained (a = 8.7 Å, b = 7.6 Å, c = 12.5 Å) agree well with the experimental data.

The eigenvectors obtained by diagonalizing the dynamical matrix were subjected to symmetry analysis. We constructed the complete vibrational representation

Table 2. Calculated parameters of the interionic interactions in crystal KPb_2Cl_5

Parameter	K^+	Pb^{2+}	Cl^-
R_W, Å	1.85	1.85	1.16
α_d, Å^3	0.7	1.6	3.3
α_q, Å^5	0.9	1.5	5.8

Table 3. Experimental and calculated frequencies of Raman-active lattice vibration modes in crystal KPb_2Cl_5

A_g, ω, cm^{-1}		B_g, ω, cm^{-1}	
calculation	experiment	calculation	experiment
34i		38i	
26i		28i	
25i		6	
21	18	28	33
34	27	39	40?
41	35	45	42
45	43	46	48
53	50	57	57
57	56	64	
58		67	
60	62	71	
67		74	75
73	73	80	85
76		84	
86	85	90	88
91		95	95
92		100	
101		103	108
106	108	107	119
110	120	115	132
123	124	120	144
129	127	129	158
134	132	140	173
159	200?	161	202

Table 4. BAW velocities in a KPb_2Cl_5 single crystal (experiment)

No.	Propagation direction	Wave type	Polarization	Velocity, m/s
1	[001]	*QL*	[001]	2766.2
2		*SS*	[010]	1520.8
3		*QSF*	[100]	1532.6
4	$\left[\frac{1}{\sqrt{2}}\ \frac{1}{\sqrt{2}}\ 0\right]$	*QL*	$\left[\frac{1}{\sqrt{2}}\ \frac{1}{\sqrt{2}}\ 0\right]$	3027.4
5		*QSS*	$\left[\frac{-1}{\sqrt{2}}\ \frac{1}{\sqrt{2}}\ 0\right]$	1442.5
6		*QSF*	[001]	1529.1
7	[010]	*L*	[010]	2717.8
8		*SF*	[001]	1731.3
9		*SS*	[100]	1521.0
10	$\left[\frac{1}{\sqrt{2}}\ 0\ \frac{1}{\sqrt{2}}\right]$	*QL*	$\left[\frac{1}{\sqrt{2}}\ 0\ \frac{1}{\sqrt{2}}\right]$	2894.0
11		*QSS*	$\left[\frac{-1}{\sqrt{2}}\ 0\ \frac{1}{\sqrt{2}}\right]$	1464.6
12		*SF*	[010]	1610.2
13	[100]	*QL*	[100]	3010.3
14		*QSS*	[001]	1532.8
15		*SF*	[010]	1730.6
16	$\left[0\ \frac{1}{\sqrt{2}}\ \frac{1}{\sqrt{2}}\right]$	*QL*	$\left[0\ \frac{1}{\sqrt{2}}\ \frac{1}{\sqrt{2}}\right]$	2778.9
17		*QSS*	$\left[0\ \frac{-1}{\sqrt{2}}\ \frac{1}{\sqrt{2}}\right]$	1471.5
18		*QSF*	[100]	1637.7

$P(g)$ of the crystal space group, which was used to calculate the projection operators [11]:

$$\Gamma_\rho = \frac{N(\rho)}{N(g)} \sum_{g \in G} \chi_\rho(g)\Gamma(g), \qquad (4)$$

where $N(\rho)$ is the dimension of the representation ρ of point symmetry operation, $N(g)$ is the dimension of the symmetry group, $\chi_\rho(g)$ is the character of the matrix of the irreducible representation ρ, $\Gamma(g)$ is the vibrational representation of the symmetry operation of the irreducible representation ρ of group G, and Γ_ρ is the projection operator. Summation is taken over all symmetry-group operations. A vibration eigenvector **f** is transformed according to the irreducible representation ρ of group G if it satisfies the criterion [11]

$$\Gamma_\rho \mathbf{f} = \frac{N(g)}{N(\rho)}\mathbf{f}. \qquad (5)$$

This algorithm of expansion of the eigenvectors of the dynamical matrix in terms of irreducible representations was realized using the Mathematica 4.2 software package.

The experimental and calculated frequencies of the Raman spectrum are given in Table 3. Note that these experimental and calculated frequencies agree well in the middle portion of the spectrum. For the lowest frequencies (below 20 cm^{-1}), the calculated frequencies depend strongly on small changes in the atomic coordinates; their variation within the experimental error can result in significant (up to 100%) changes in the vibration frequencies.

Figure 4 shows the relative contributions of the atomic displacements to the eigenvectors of the corresponding modes (the renormalization to ionic masses was taken into account). To check the correctness of the procedure, we calculated the atomic displacements for

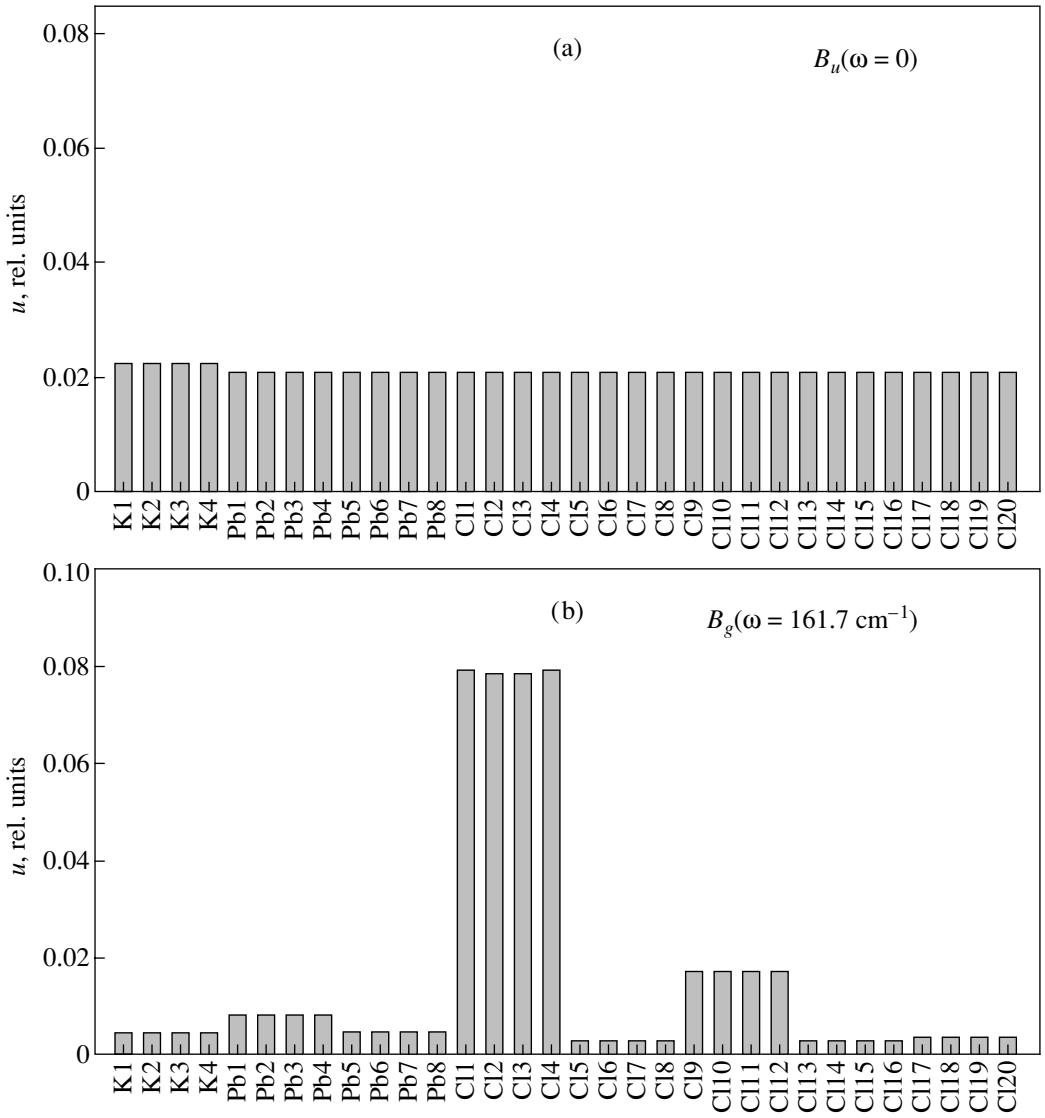

Fig. 4. Relative ion-vibration amplitudes of (a) the acoustic mode, (b) high-frequency mode, and (c) low-frequency mode. (d) The relative ion-vibration amplitude of a middle-range Raman-active mode. (e) The relative ion-vibration amplitude of a Raman-inactive polar mode.

the acoustic mode. The results support the correctness and are shown in Fig. 4a. Figure 4b shows the atomic displacements for the highest frequency spectrum mode, which corresponds to the spectral-window boundary of the crystal. It is seen that, although the maximum displacements correspond to chlorine ions, the contribution of heavy metal ions to the eigenvector of this vibration remains significant, which is likely to account for the relatively low value of the corresponding frequency (as compared, e.g., to the frequencies in high-symmetry perovskite-like chloride systems [15]).

As is seen in Figs. 4c–4e, the low symmetry of the structure leads to a strong interaction between the vibrations of atomic sublattices in virtually all vibration modes; in particular, even the lowest frequency modes contain a significant contribution from the displacements of light chlorine ions.

3.2. Elastic Moduli

The problem of determining the elastic moduli $C_{\lambda\mu}$ by measuring the BAW velocities for monoclinic media was solved in [12] and discussed in detail in [13]. In the chosen crystallographic setting, the elastic-modulus matrix of the crystal has the form [14]

$$\begin{pmatrix} C_{11} & C_{12} & C_{13} & 0 & C_{15} & 0 \\ C_{12} & C_{22} & C_{23} & 0 & C_{25} & 0 \\ C_{13} & C_{23} & C_{33} & 0 & C_{35} & 0 \\ 0 & 0 & 0 & C_{44} & 0 & C_{46} \\ C_{15} & C_{25} & C_{35} & 0 & C_{55} & 0 \\ 0 & 0 & 0 & C_{46} & 0 & C_{66} \end{pmatrix}. \quad (6)$$

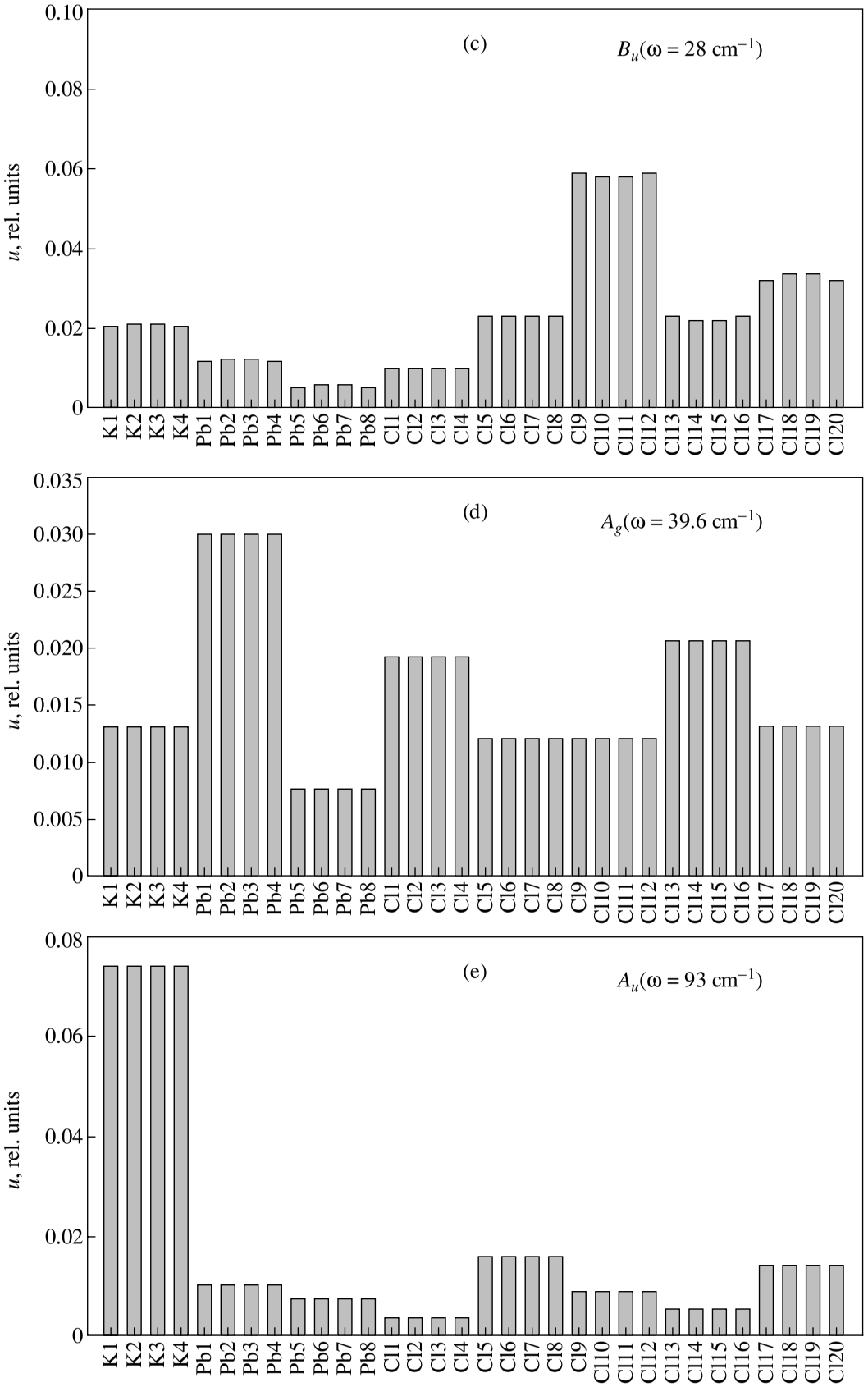
(c)
$B_u(\omega = 28\ \mathrm{cm}^{-1})$
(d)
$A_g(\omega = 39.6\ \mathrm{cm}^{-1})$
(e)
$A_u(\omega = 93\ \mathrm{cm}^{-1})$
u, rel. units
0.10
0.08
0.06
0.04
0.02
0
0.035
0.030
0.025
0.020
0.015
0.010
0.005
K1 K2 K3 K4 Pb1 Pb2 Pb3 Pb4 Pb5 Pb6 Pb7 Pb8 Cl1 Cl2 Cl3 Cl4 Cl5 Cl6 Cl7 Cl8 Cl9 Cl10 Cl11 Cl12 Cl13 Cl14 Cl15 Cl16 Cl17 Cl18 Cl19 Cl20

Fig. 4. (Contd.)

Table 5. Experimental and calculated elastic moduli of crystal KPb_2Cl_5 (in units of 10^{10} N/m^2)

Elastic modulus	C_{11}	C_{12}	C_{13}	C_{15}	C_{22}	C_{23}	C_{25}	C_{33}	C_{35}	C_{44}	C_{46}	C_{55}	C_{66}
Experiment	4.34	1.93	1.77	–0.55	3.53	1.52	0.05	3.62	0.06	1.11	0.03	1.10	1.43
Calculation	4.00	1.30	1.37	–0.03	3.87	1.42	0.01	3.47	0.01	1.30	0.03	1.30	1.24

The independent elastic moduli were separately determined using the method of special directions [12, 13]. The measured BAW velocities and the main BAW characteristics are given in Table 4. The experimental error in determining the BAW velocities was less than 0.5 m/s.

The elastic moduli $C_{\lambda\mu}$ are calculated from the known eigenvalues ρv^2 of the Green–Christoffel tensor [13] $\Gamma_{\alpha\gamma} = C_{\alpha\beta,\gamma\delta}n_\beta n_\delta$ by solving the Green–Christoffel equations $(\Gamma_{\alpha\gamma} - \rho v^2\delta_{\alpha\gamma})U_\delta = 0$ for each crystallographic direction. Here, $\rho = 4.780$ g/cm^3 is the density of the crystal under study; v is the velocity of BAW with polarization U_δ; n_α are the direction cosines of the wave normal; and $C_{\alpha\beta,\gamma\delta}$ is the elastic-modulus tensor, whose components are related to the elastic-modulus matrix $C_{\lambda\mu}$ by the well-known Voigt transformation [14].

The elastic moduli of the single crystal are calculated using the procedure described in [12, 13] and are given (in units of 10^{10} N/m^2) in Table 5, which also presents the elastic moduli calculated in the Gordon–Kim model. For centrosymmetric crystals, the elastic moduli are related to the dynamical matrix of a crystal by the expressions [6]

$$C_{\alpha\beta,\gamma\delta} = [\alpha\beta,\gamma\delta] + [\gamma\beta,\alpha\delta] - [\alpha\gamma,\beta\delta],$$
$$[\alpha\beta,\gamma\delta] = \frac{1}{2V}\sum_{k,k'=1}^{N_a}\sqrt{m_k m_{k'}}D^{\gamma\delta}_{kk',\alpha\beta}, \quad (7)$$

where V is the unit cell volume, k and k' are the ion indices, N_a is the number of ions in the unit cell, m_k is the ion mass, and

$$D^{\gamma\delta}_{kk',\alpha\beta} = \left.\frac{\partial^2 D_{kk',\alpha\beta}}{\partial q_\gamma \partial q_\delta}\right|_{q=0}$$

are the coefficients of expansion of the dynamical matrix D in powers of the wave vector **q** for the second-order term.

A comparison of the experimental and calculated values shows that they agree well with each other.

4. CONCLUSIONS

We have recorded the polarized Raman spectra of KPb_2Cl_5 crystals and interpreted them using a parameter-free model with inclusion of the higher multipole moments of ions of the crystal lattice. The model developed has been shown to provide good agreement between the calculated and experimental frequencies of the vibrational spectrum of the low-symmetry ionic crystal with a complex structure. The eigenvectors of lattice vibrations were determined and analyzed. It was found that the frequencies of the phonon spectrum are low due to the significant (although small) contribution of heavy cations even to the eigenvectors of the highest frequency vibration modes.

Using the same approach, we have experimentally and theoretically determined the elastic moduli of the crystal and achieved good agreement between the experimental and calculated values.

ACKNOWLEDGMENTS

The authors thank V.I. Zinenko for helpful discussions of the results.

This work was supported by the integration program of the Siberian Division, Russian Academy of Sciences (project no. 88), the program of support for leading scientific schools (project no. NSh-939.2003.2), and the programs of the Presidium of the RAS and of the Department of Physical Sciences of the RAS.

REFERENCES

1. K. Nitsch, M. Dusek, M. Nikl, K. Polak, and M. Rodova, Prog. Cryst. Growth Charact. Mater. **30**, 1 (1995).
2. R. Balda, J. Fernandez, A. Mendioroz, M. Voda, and M. Al-Saleh, Phys. Rev. B **68**, 165101 (2003).
3. O. V. Ivanov, D. A. Shport, and E. G. Maksimov, Zh. Éksp. Teor. Fiz. **114**, 333 (1998) [JETP **87**, 186 (1998)].
4. N. G. Zamkova, V. I. Zinenko, O. V. Ivanov, E. G. Maksimov, and S. N. Sofronova, Ferroelectrics **283**, 49 (2003).
5. A. N. Vtyurin, S. V. Goryaĭnov, N. G. Zamkova, V. I. Zinenko, A. S. Krylov, S. N. Krylova, and A. D. Shefer, Fiz. Tverd. Tela (St. Petersburg) **46**, 1261 (2004) [Phys. Solid State **46**, 1301 (2004)].
6. M. Born and K. Huang, *Dynamical Theory of Crystal Lattices* (Clarendon, Oxford, 1954; Inostrannaya Literatura, Moscow, 1958).
7. M. B. Smirnov, in *Dynamic Theory and Physical Properties of Crystals*, Ed. by A. N. Lazarev (Nauka, St. Petersburg, 1992), p. 41 [in Russian].

8. A. A. Merkulov and L. I. Isaenko, in *Proceedings of the V International Conference on Crystals: Growth, Properties, Real Structure, Application* (Aleksandrov, 2001), p. 83.
9. A. A. Merkulov and L. I. Isaenko, Zh. Strukt. Khim. **45**, 724 (2004).
10. B. P. Sorokin, P. P. Turchin, and D. A. Glushkov, Fiz. Tverd. Tela (St. Petersburg) **36**, 2907 (1994) [Phys. Solid State **36**, 1545 (1994)].
11. H. Streitwolf, *Gruppentheorie in der Festkörperphysik* (Teubner, Leipzig, 1967; Mir, Moscow, 1971).
12. K. S. Aleksandrov, Kristallografiya **3**, 639 (1959) [Sov. Phys. Crystallogr. **3**, 647 (1959)].
13. K. S. Aleksandrov and G. T. Prodaĭvoda, *Anisotropy of Elastic Properties of Minerals and Rocks* (Sib. Otd. Ross. Akad. Nauk, Novosibirsk, 2000) [in Russian].
14. Yu. I. Sirotin and M. P. Shaskolskaya, *Fundamentals of Crystal Physics* (Nauka, Moscow, 1975; Mir, Moscow, 1982).

Translated by K. Shakhlevich